

Document downloaded from:

<http://hdl.handle.net/10251/105462>

This paper must be cited as:

Tormos, B.; Ramirez-Roa, LA.; Johansson, J.; Bjorling, M.; Larsson, R. (2017). Fuel consumption and friction benefits of low viscosity engine oils for heavy duty applications. *Tribology International*. 110:23-34. doi:10.1016/j.triboint.2017.02.007



The final publication is available at

<https://doi.org/10.1016/j.triboint.2017.02.007>

Copyright Elsevier

Additional Information

Fuel Consumption and Friction Benefits of Low Viscosity Engine Oils for Heavy Duty Applications.

Abstract


One of the most attractive ways to tackle vehicle engine's inefficiencies is the use of Low Viscosity Engine Oils (LVEO). Adopted some decades ago for their use in the Light Duty segment, LVEO are now reaching the Heavy Duty segment.

In this study, a comparative fuel consumption test, where a LVEO performance is evaluated on an urban compressed natural gas buses fleet is portrayed. Then the friction performance of the same oils are studied on a Cameron-Plint tribometer, on an adapted twin disc tribometer to simulate journal bearing friction and on a Ball-on-Disc rig, using real engine parts in the former and the same set of engine oils used during the fleet test.

Results show a fuel consumption reduction in the fleet test and corresponding friction reduction in the tribometers when LVEO are used.

Keywords: Low Viscosity Engine Oils, Engine friction losses, Piston-assembly, Valve-train

Highlights

- Low viscosity engine oils tested in fleet and laboratory.
 - The use of low viscosity oils (LVEO) led to reduced friction coefficient in the tribo-contacts of the engine.
- 

- The reduction of friction coefficient in these tribo-contacts will be translated into fuel consumption benefits.
- The friction reduction found in the Cameron-Plint Test, Journal Bearing Test Rig and the WAM machine are consistent with the fuel consumption decrease during the fleet test when LVEO were used.

1. Introduction

The CO₂ emissions and fuel consumption reduction has arisen as a key driver in the automotive industry R&D, linked to a general public concern over Global Warming and the Green House Effect caused partially by the Green House Gases emitted by the vehicles which use Internal Combustion Engines as powertrain.

This concern has led to more restrictive CO₂ emissions standards in a vast number of industrialized countries. Although these regulations have been set for light duty passenger cars initially, the oncoming trend is to embrace Heavy Duty Vehicles (HDV) as well. It has to be mentioned that research in the HDV segment during the last years has been dedicated to reduce pollutant emissions, especially HC, CO, NO_x and particulate matter; this trend is evident when the progression limits of the Euro emission standards is analyzed[1].

From the cycle energy break down of a HDV, it is evident that most of the energy that comes from the fuel is used to overcome the different losses in the vehicle. Several energy distributions for HDV have been proposed by different authors where the type of vehicle and its duty cycle are the main factors defining those distributions. Holmberg et al, have proposed the

energy break down for urban buses where 51 % of energy is lost in exhaust and cooling, 18.5 % in engine and transmission friction and 5.5 % in auxiliary loads leaving just 25 % of the initial energy contained in the fuel to move the vehicle[2].

An obvious approach to reduce the CO₂ emissions is to tackle the different sources of vehicle losses. One proven cost-effective way to increase engine efficiency is the use of Low Viscosity Engine Oils (LVEO) in order to reduce the friction losses in engine tribo-contacts which represent nearly 10 % of the total losses, making them a good target in order to enhance engine efficiency, hence reducing CO₂ emissions. To understand how the use of LVEO could enhance engine efficiency it is crucial to understand engine friction and lubrication. In every pair of elements sliding against each other with relative motion exists a force acting against this movement, that force is friction, which depending on the lubricated pair characteristics will require more or less work to be overcome. The relationship between the lubricated pair and the friction coefficient is described by the Stribeck curve[3]; the curve shows the friction coefficient behavior for all the lubrication conditions, depending mainly on the lubricant rheology (specifically on lubricant viscosity η), the relative speed between the moving parts (U) and the normal force held by the parts (F). From the Stribeck curve three main lubrication regimes can be distinguished: the first one, where the lubricant layer between the parts in relative motion does not hold any load by hydrodynamic effects, allowing direct contact between the parts, which is called Boundary Lubrication Regime. The second one where the lubricant film layer is fully developed and the main

Interface	Hydrodynamic	EHD	Mixed	Boundary
Piston assembly (5.5 %)	2.2 %	2.1 %	0.6 %	0.6 %
Journal Bearings (3 %)	3 %	-	-	-
Valve Train (1.5 %)	-	-	1.5 %	-

Table 1: Distribution of the engine friction losses by lubrication regimes for a bus (year 2000, bus @ 20 km/h).

resistance is given by the lubricant inner friction is known as the Hydrodynamic Lubrication Regime. A mixture of the previous two with miscellaneous characteristics of boundary and hydrodynamic regimes along the contact interface is called mixed lubrication. Specifically for ICE, several authors[4–6] have studied the friction distribution among the most important lubricated engine pairs: the piston-cylinder liner, followed by the bearings and finally the engine distribution system. Holmberg et al. have proposed a distribution of lubrication regimes for these three lubricated pairs, this time focused on the urban buses, the type of vehicle which is interesting for this study (see table 1.)

1.1. Piston ring pack interface

As it can be seen, nearly a 6 % of total vehicle losses are present at the piston ring pack interface, most of it under hydrodynamic lubrication regime. This fact opens the possibility to reduce friction coefficient only by reducing oil viscosity. This effect has been measured by several authors in terms of fuel consumption reduction particularly for the passenger cars segment[7–13], however this focus has been changing and some studies have addressed the effect of LVEO on HDV efficiency improvement.[5, 14–18]

Some of these studies have used reciprocating rigs to simulate the piston ring dynamics and loads over the cylinder in order to find the friction coefficient behavior, both using laboratory specimens or real engine parts[19–30].

1.2. Journal bearings

This tribo-contact is the second source of engine friction as seen in table 1. Although Journal Bearings could work under boundary and mixed regimes owing to changes in loads, speeds, and temperature [31], during engine operation this friction occurs under hydrodynamic lubrication regime. As for piston assembly, the use of LVEO could reduce losses in this interface, however, as these losses are decreased by reducing lubricant viscosity, the appearance of metal-metal contact becomes more likely, hence in recent years the study of bearing materials, coatings, transient loads and their respective wear performance have been widely studied[31–34].

1.3. Valvetrain

There are several cam-follower configurations where push-rod cam-followers is the most used for large HDV engines. The main frictional losses in the valve train occur between the cam and the tappet, the tappet and its bore, the rocker arm bearing, the valve stem and the valve guide and in the camshaft bearings. However, in terms of total energy, the energy dissipated in the cam and the tappet interface usually rises up to the 85 % of the total energy dissipated in the valvetrain[35, 36], hence the importance to study how the LVEO behaves in this interface. The valve train works normally under the hydrodynamic and elastohydrodynamic

(EHD) lubrication regimes[37]; the former on the base of the cam circle and the latter case when the contact point is in the vicinity of the cam nose.

1.4. Use of LVEO on Heavy Duty Vehicles

The adoption of LVEO in the Heavy Duty Vehicles segment has lagged behind the passenger cars segment, due to a concern about their capability to withstand the loads associated with heavy duty cycles. However, in the recent years and following the general trend to reduce fuel consumption and CO₂ emissions of the automotive industry, new Heavy Duty Engine Oil categories were proposed by API (the American Petroleum Institute) in order to reach gains in fuel consumption benefits. On December 2016, API introduced two engine oil categories, CK-4 and FA-4, the former having a backward compatible role with previous category CJ-4 and the latter dedicated to increase vehicles fuel economy, surpassing the historic High Temperature High Shear viscosity (HTHS) limit of 3.5 cP. In Europe however, the recent ACEA engine oil specifications played it safe keeping the HTHS value in 3.5 cP[38].

2. Experimental methodology

For this study, fuel consumption data from a previous fleet experiment have been taken to be complemented with friction coefficient variation data from laboratory test rigs. The methodology used for laboratory tests was simple: to compare the friction coefficient in the tribo-contacts using the same engine oils used during the fleet test. The specific procedures are explained below.

Characteristic	CNG Vehicle
Year	2007
Length / width / height [m]	12/2.5/3.3
Engine displacement [cm^3]	11967
Cylinders	6
Max. effect power [kW]	180 @ 2200 [1/min]
Max. effect torque [Nm]	880 @ 1000 [1/min]
Crankcase volume [l]	33
BMEP [bar]	9.24 @1000 [1/min]
Thermal load [W/mm^2]	2,33
Valve train config.	OHV Push-rod Cam Follower

Table 2: CNG buses characteristics

2.1. Fleet test

The fleet test data have been taken from a fuel consumption study where CNG buses of the same model working under real conditions were divided in two groups; one using a SAE 10W40 Low SAPS engine oils as a baseline and another using a SAE 5W30 Low SAPS acting as Low Viscosity Engine Oil (LVEO)[39]. All buses worked during two Oil Drain Intervals (ODI) of 30000 km each, and fuel consumption data were calculated daily from mileage and consumed fuel. Buses characteristics can be seen in table 2.

2.1.1. Baseline and Low viscosity engine oils

The oils used during this test as LVEO and baseline oil can be seen in table 3. Both oils were commercial available.

Oil	10W40 Low SAPS	5W30 Low SAPS
Used as	Reference	Candidate
Base oil	API G-III	API G-III + G-IV
kV@40°C [cSt]	96	68
kV@100°C [cSt]	14.4	11.7
HTHS@150°C [cP]	3.853	3.577
VI	≥ 145	≤ 169

Table 3: Oils characteristics

2.2. Cameron-Plint machine TE77

The Cameron-Plint TE77 is a reciprocating test rig, which could use piston rings and cylinder liner specimens from real engine parts in order to mimic the contact inside the combustion chamber of the piston assembly of an internal combustion engine. The machine comprises an upper holder where the piston ring is mounted. This holder moves against a fixed specimen of the cylinder liner placed in the bottom holder which is fixed in an oil bath to ensure oil-flooded conditions when required (see Figure 1). The test rig allows changing the normal force from 0 N to 250 N applied directly over the upper holder. An electric motor and an eccentric cam produce the reciprocating movement enhancing the possibility to control the linear speed through the motor frequency and the stroke length. The stroke length was fixed at 8 mm, the maximum value permitted by the rig, and the minimum and maximum frequencies were 1Hz and 7Hz respectively. A piezoelectric transducer measured the friction force along the reciprocating direction.

The measurements were focused on the oil control ring (OCR) which is

Specimen	Length [mm]	Width/Land-width [mm]
Compression Ring	80	3.5
Scraper Ring	80	3
Oil Control Ring	80	0.8
Liner	50	8

Table 4: Specimens characteristics

the one that works under oil-flooded conditions and responsible for a major part of the losses of the piston ring pack.

Oils used during the measurements were fresh and their temperature was controlled in order to maintain the viscosity steady during the tests. Piston ring and liner conformability was checked using pressure film before each test. A running-in procedure, for piston ring and cylinder liner specimens was done before each measurement. The process is similar to the one used by Truhan et.al. with a low frequency (1Hz) and high load (250 N) during 60 minutes[20]. In a similar way, an oil washing procedure comprising 60 minutes at 250 N and 1 Hz was made with the oil to be tested.

2.2.1. Test specimens

The specimens tested in the reciprocating rig were taken from real Heavy Duty spare parts. This engine corresponded to the reference used in the CNG buses with a nominal bore diameter of 128 mm. Table 4 shows the geometric characteristics of the ring and cylinder liner specimens used during the test.

Test	Screening	Reverse stroke
Points	9	7
Repetitions	3	3
Oils	5W30 & 10W40	5W30 & 10W40
Load [N]	20, 70 and 150	10
Frequency [Hz]	1, 3, 7	1-7

Table 5: Test points for the Cameron-Plint machine tests.

2.2.2. Test points

Two different tests were performed in the Cameron-Plint machine: one screening test varying load and relative speed in order to identify the most beneficial conditions to reduce friction coefficient of the piston ring-cylinder liner pack, similarly to the approach used by Spencer et.al.[25]. In the second test the load was fixed to the required value to achieve the Nominal Contact Pressure values given in Table 6. However, a 10 N load was used instead to assure repeatability. This second test could be interpreted as a reverse piston stroke, where loads and relative speeds are very low. The test points are described in the table 5.

2.2.3. Nominal contact pressure of the piston ring pack

The tension for the compression and scraper ring was taken from other rings with the same bore diameter. From these values, the nominal contact pressure was derived from expression 1:

$$P_o = \frac{2F_t}{d_n h_c} \quad (1)$$

Where F_t is the ring tension, d_n is the bore nominal diameter and h_c

Ring	OCR	Scraper	Compression
d_n [mm]	128	128	128
h_c [mm]	0.8	3	3.5
P_o [$\frac{N}{mm^2}$]	1.22	0.133	0.167
F_t	62.5	25.6	37.3
Area [mm^2]	6.4	24	28
F [N]	7.8	3.2	4.7

Table 6: Ring pack characteristics, nominal contact pressure, specimen characteristics and normal force to be applied in the Cameron-Plint machine.

is the piston ring land width. In the case of the oil control ring (OCR), the nominal contact pressure value was taken from the JSAE 2003[40]. The complete characteristics for the ring pack can be seen in Table 6.

2.3. Journal Bearing Test Rig

This in-house built device was used to analyze the friction performance of the engine oils in journal bearings, such as the crankshaft main bearings. The basics of the setup can be seen in Figure 2. A 20.5 mm wide, 53 mm diameter shaft is simulating a crankshaft journal, which is clamped to a drive spindle, driven by a servomotor with adjustable speed, up to 3000 min^{-1} . The setup also includes a self-aligning bearing holder that is used to mount two bearing sleeves. The upper bearing sleeve contains an oil groove to distribute oil from an oil inlet. Both upper and lower sleeve bearing specimens were commercially available and had a steel backing and an aluminum based lining material as described in Table 7. Load is applied by the use of dead weights that through a lever mechanism forces the spindle (and journal) towards the

Element	mass [%]
Al	84.0
Sn	12.0
Si	3.0
Cu	1.0

Table 7: Composition of journal bearing lining

lower bearing with a force of up to 2000 N. Friction is obtained by measuring the torque required to rotate the journal.

The oil volume used for each test was 2.0 L. Prior pumping, the oil passes through a strainer (125 μm), then the pressurized oil is filtered again (3 μm) before it reaches the bearing holder. This oil is injected to lubricate the bearing as well as sprayed with jets to control the holder temperature. The supply pressure at the bearing holder was 0.09 MPa and the total flow rate was 60 ml/sec . The oil temperature is measured in the oil supply line, just prior to the bearing holder. The oil temperature is maintained by a heater situated below the oil bath.

2.3.1. Test specimens

For each new test, new bearing sleeves and a new journal was mounted. For this, the journal diameter and the thicknesses of the bearing sleeves were chosen so that a diametrical clearance of 0.028 mm ($\pm 0.004 \text{ mm}$) was obtained in each test. The width of the bearing sleeves were 20.0 mm . The journals were made out of commercial steel (16NiCrS4) that was case-hardened and tempered to a surface hardness of 55 HRC. The hardened disc specimens were then ground on the outer surface and most non-contact

surfaces. Special attention was given to the discs' outer diameter surface, as it needed to be representative of automotive crankshafts. For this, a grinding method producing a circumferentially orientated surface lays was used. The surface roughness of the new discs was measured to 65 nm (Ra).

2.3.2. Test procedure and test points

Each test was started by increasing the oil temperature to $80 \text{ }^\circ\text{C}$; once the temperature was reached, the rotation of the journal was started and brought up to 3000 min^{-1} . Once the speed of 3000 min^{-1} was reached, a load of 2000 N was applied. The rig was maintained under these conditions for a 30 min period in order to achieve temperature stabilization.

The remainder of a test consisted of 10 sweeps through a range of speeds in order to plot "Stribeck type" friction curves with boundary lubrication at low speeds and full film hydrodynamic lubrication at high speeds. At 12 points in each sweep, the friction was measured by maintaining a fixed rotational speed for 10 seconds in order to get an average value at that point.

Between each sweep, the rotational speed of the journal was fixed at 3000 min^{-1} for 5 minutes to allow the temperatures to stabilize. With each sweep, the contacting surfaces will have been more run-in, showing how it affects the oils' performance. For each oil, 3 individual tests were performed and the averages of the 3 tests were used.

2.4. WAM machine

The ball-on-disc friction measurements were conducted in a Wedeven Associates Machine (WAM) device. As described in Bjorling et.al.[41] this device use a ball loaded against a solid disc resulting in a circular EHD

contact. The tribometer has a constant oil supply from the center of the disc and the rotation of both, ball and disc, drags the lubricant into the contact where a lubricant layer is formed. The ball and the disc rotatory movements are driven by two independent electric motors, the former to a speed up to 25000 rpm and the latter up to 12000 rpm (see Figure 3).

From the test geometric configuration and rotational speeds, the ball linear speed U_b and the disc linear speed at the contact U_d can be calculated. From those speeds the lubricant entrainment speed is given by the equation 2.

$$U_e = \frac{U_b + U_d}{2} \quad (2)$$

As the rotational speed of ball and disc are independent, different linear speeds at the ball and disc contact can be achieved, resulting in rolling and sliding contact. The Slide to Roll Ratio is defined by the equation 3.

$$SRR = \frac{U_b - U_d}{U_e} \quad (3)$$

Load cells are used to measure the force on the three principal axes and to calculate the contact friction coefficient.

2.4.1. Test points

The ball on disk test device was used to generate friction data from a series of tests under different operating conditions. The tests were performed with three different entrainment speeds; 1, 2.5 and 4 m/s. In each test cycle, the entrainment speed was held constant while the slide to roll ratio was varied from 0.0002 to 1.05. All tests in this investigation were hence conducted

with the ball having a higher surface speed than the disk. Both ball and disk specimens were cleaned with heptane and ethyl alcohol before starting the experiments for each of the test cases. All tests were performed with a load of 300 N which corresponds to a maximum Herzian pressure of 1.94 GPa, a common value for valvetrain systems in Heavy duty engines [36, 42–45]. The tests were performed at two different temperatures; 40 and 80°C, and with the two different lubricants used in the bus fleet test, described in Table 3. Before starting the experiments for each test case, the test device was warmed up to the desired operating temperature for approximately 60 minutes with lubricant circulation over both ball and disk to ensure thermal stability. When a stable temperature was reached, a 300 N load was applied and the machine was calibrated for pure rolling by adjusting spindle angle and positioning of the ball to ensure a condition of no spinning. These settings were then held constant for 20 minutes to ensure a mild run-in. Subsequently, the test cycle was started, wherein the load and entrainment speed were kept constant, and slide to roll ratio were varied from the lowest to the highest value. The temperature of the oil bulk and fluid adhered to the disk surface was typically deviating less than $\pm 1.5^\circ\text{C}$ from the target temperature of 40 and 80 °C during testing. The complete description of the test conditions is shown in the table 8.

3. Results & discussion

3.1. Fleet test

After carrying out the 60000 km mileage, the buses that used SAE 5W30 Low SAPS gave a fuel consumption of 85.1 Nm³/100 km,

Parameter	Values
Entrainment speed [m/s]	1, 2.5, 4
Slide to Roll Ratio	0.0002 to 1.05
Pressure (GPa)	1.94
Temperature [°C]	40, 80
Oils	Low and High viscosity

Table 8: Test points for the WAM - Machine test

Factor	Sum of Squares	Degrees of Freedom	P-Value
Daily Temp [°C]	670.4	1	0.048
Oil mileage [km]	13561.0	1	0.006
Engine Oil	16733.1	1	0.004
Route	375386.0	1	0.000
Month	4850.19	11	0.0125

Table 9: ANOVA results for CNG buses.

considerably lower than the 88.37 Nm³/100 km of fuel consumption given by the buses using SAE 10W40 Low SAPS. For CNG buses this difference of 3.7 % is statistically significant, demonstrating the benefits of using LVEO in terms of fuel consumption. The effects of other variables like atmosphere conditions, weather seasonality, load and route characteristics were characterized by means of an ANOVA analysis. The complete results can be seen in table 9 and Figure 4.

The complete results of this test, including the CO₂ emission equivalence can be seen in Macián et. al. [39].

3.1.1. *Studies on wear, oil consumption and its relation with LVEO use.*

Even when it is not the main objective of the present study, it is worth to mention the wear performance during the fleet test. One of the main concerns about the use of LVEO in the Heavy Duty segment is the chance of increased rates of wear due the thinning of the lubricant layer and consequently, its capacity to withstand loads under the demanding conditions of the duty cycles.

Macián *et.al.* analyzed wear metals from oil samples taken each 3000 km from the CNG buses, both for LVEO and the reference oil. Data did not show evidence of wear or oil consumption increase from the use of LVEO[46].

These results corroborate the fuel consumption benefits reported by NACFE when engine oils with a 5W30 over 10W40 SAE viscosity grade were used in HDV fleets. In the same way, the good results regarding wear performance during the test done by Macián *et.al.*, validate as well the high confidence rating given for this type of oils by NACFE in its 2016 confidence report[47].

3.2. *Cameron-Plint TE77 results*

As stated in section 2.2 two different tests were performed with the Cameron-Plint machine: one screening test varying the oil, load and stroke frequency (average speed) using only the Oil Control Ring (OCR) and another with the three piston rings, compression, scraper and OCR working at a load similar to those found during the piston reverse stroke and varying the stroke frequency. To plot the resulting Stribeck curves from the test, the Sommerfeld number was used as reference for the different friction coefficient values. The Sommerfeld number is given by the expression 4

where η is the oil dynamic viscosity, U is the relative speed and P is the contact pressure.

$$S = \frac{\eta U}{P} \quad (4)$$

Given the fact that friction measurements were made at low temperatures in order to avoid the consequent engine oil viscosity drop, the actual viscosity value was calculated with the mean temperature at each test point and the Vogel equation 5 which is the most used approximation in engineering calculations[48]. The equation coefficients were found based on previous viscosity measurements at 40°C 100°C and 150°C following ASTM D5481[49, 50].

$$\eta = ae^{\frac{b}{(T-c)}} \quad (5)$$

3.2.1. Screening test

The results of the screening test can be seen in table 10 and in Figure 5. The ANOVA shows that the three main effects under study have a significant effect on the friction coefficient since the p -value is less than 0.05.

From the results of ANOVA it is possible to state that the use of SAE 5W30 engine oil instead of SAE 10W40 in this tribo-contact reduced the friction coefficient by 4.24 %. In the same way, the increase of normal load had the greatest impact over the friction coefficient: An increase from 20 N to 150 N produced a 33.51 % decrease of the friction coefficient. Lastly, the variation of entrainment speed was shown to have a significant effect on friction coefficient having a difference of 15.13 % between the slowest and

Main effects	Sum of Squares	Degrees of Freedom	p -value
A: Oil	0.000076	1	0.0385
B: Load	0.004365	2	0.0001
C: Frequency	0.000729	2	0.0019
Interactions			
CB	0.000058	4	0.2949
AC	0.000009	2	0.6162
BA	0.000026	2	0.3134
Residues	0.000033	4	
Total	0.005295	17	

Table 10: ANOVA results for the screening test

the fastest entrainment speed. It has to be stated that the role of load in the Cameron-Plint test seems to be predominant (as can be seen in table 10). However, compared to the real situation in the engine, the contact pressure values of the rings (directly related to normal forces in the Cameron-Plint) and the relative speed exhibit opposite scenarios: 20 N to 150 N over the contact area represent nominal contact pressures of 3.125 N/mm² to 23.44 N/mm². Despite the fact this screening test was done over the OCR, these contact pressure values could be present in compression and scraper rings during engine operation. *Per contra*, the relative speeds reached in the Cameron-Plint are distant from the actual engine speeds, and from the engine point of view all the three values used as input in the rig are relatively low and close to speeds found at top and bottom dead centers (TDC and BDC).

3.2.2. Piston rings under reverse stroke conditions

As described in section 2.2, the aim of this test was to mimic the loading conditions of the rings at reverse conditions (that is some crank angle grades before and after the combustion). Figure 6 describes the friction coefficient behavior against the Sommerfeld number for the three piston rings and the two oils. It should be noticed that the scale on the x-axis decrease for each piston ring, following the contact pressure values given in Table 4 and the Sommerfeld number (Equation 3). The higher contact pressure value of the OCR correlates precisely with the higher values of friction coefficient, which decrease slightly as the speed increases (as part of the Sommerfeld number the load and viscosity are fixed for this test) in contrast with the notorious decline of friction coefficient as the relative speed increases for the compression and scraper ring. As a general trend the friction coefficient curves have moved towards the left. This outcome can be interpreted in two ways: in most of cases for a given Sommerfeld number (that is the relation between lubricant viscosity, relative speed and contact pressure) the friction coefficient value declines, hence the friction force is going to decrease using the less viscous oil. On the other hand, it is not possible to say that for every fixed values of load and relative speed, the friction coefficient will drop by the use of an oil with lower viscosity. Having the Stribeck curve moved to the left the boundary and mixed regimes could be found easier if the oil layer could not hold the applied load (as at high speeds in the case of piston rings of Figure 6).

3.2.3. Factor interactions on the Cameron-Plint screening test

In addition to the fact that results in Figure 5 are useful to determine the sensibility of friction coefficient, it is of special interest to determine how the load and the relative speed affects the low viscosity oil capacity to reduce fuel consumption. In Figure 7, the combined effects of load and relative speed over the friction coefficient are depicted. It is clear that for every measured relative speed, friction coefficient drops sharply as the load increases from 20 N to 150 N. This trend is somehow unexpected if interpreted by the theory enclosed in the equation 4: higher loads, in this case contact pressures, should give higher friction coefficients; however, it is possible that a severe load variation as the one proposed for the screening test led to strong deformations making the contact to have independent Stribeck curves as is plotted in Figure 8.

Figure 9 depicts the friction coefficient dependence on engine oil viscosity and relative speed. It is clear that for the three measured speeds, the SAE 5W30 engine oil gives a lower friction coefficient value. However, for the lowest speeds the friction coefficient has fallen marginally in contrast to the behavior at high speed that shows a substantial decrease around to 6.73 %. This trend is somehow expected: high relative speeds favor the hydrodynamic lubrication regime precisely where the less viscous oil has a greater potential to reduce friction.

A similar situation can be seen in Figure 10 where the combined effect of oil viscosity and load over friction coefficient are shown. As expected the less viscous oil presented lower friction coefficients for the 20 N and 70 N levels of load. However, at the highest load the friction coefficient remained stable,

that is, the oil viscosity could not offer any upturn with the given conditions. Probably at this point the contact at the Cameron-Plint machine is working under the boundary lubrication regime and the reduction of the viscosity of the oil could lead to even higher friction coefficients. In fact, the friction coefficient at 150 N and 7 Hz is higher for the 5W30 oil as the Stribeck curve moves towards the left due the decrease of engine oil viscosity, behavior that was clear during the "reverse stroke" like test.

3.2.4. Friction coefficient and lubrication regime of tests

As it was observed in Figure 6, the friction coefficient value for all the conformed contacts of liner and the correspondent piston ring showed values near 0.1 that are typically associated with mixed and boundary lubrication regimes. This behavior is especially evident in the OCR that presents high friction coefficient values for all ranges of speed probably due the greater value of nominal contact pressure. On the other hand, the scraper ring, (which is the one with less nominal contact pressure) displays a clear trend towards low friction coefficients as the speed increases, typical of the mixed lubrication regime. Complementarily, it is in this ring where the greatest difference of friction coefficient between the two oil formulations can be seen. These results simply show that the relative speed was too low to ensure enough pressure in the lubricant film to separate the surfaces. That fact should be kept in mind when analysing the values of friction coefficient reduction; the Cameron-Plint results are not showing the engine mid-stroke friction coefficient but the reverse points where speed is low and the pressure in the combustion chamber does not correspond to the values near the top dead center when combustion takes place. However, it is remarkable that even with the test

rig limitations, the differences in friction coefficient at mixed and boundary regimes caused by the difference in oil viscosity can be detected.

3.3. Journal Bearing Test Rig results

The results of the journal bearing test are shown in Figure 11. In the figure, the friction coefficient for the oils under different rotational speeds for sweep 1 (A) and sweep 10 (B), and their respective friction differences in percentage (%) are shown. The figure only includes the hydrodynamic part of the curves since it is most relevant for the conditions occurring in buses engines during normal operation. These "Stribeck like" curves show the expected friction behavior, with friction coefficient values decreasing rapidly from 0.1 (not plotted) to a minimum around 0.003 to start an increase again alongside the rotational speed.

3.3.1. The effect of LVEO on friction coefficient

The results showed that at low speed, the difference in friction coefficient is almost negligible, in fact, at very low speed the LVEO results in higher friction. However, in the hydrodynamic regime the LVEO leads to a reduction of the friction coefficient for the whole speed range. For all sweeps, an 8 % friction reduction can be seen at the maximum speed. However, one noticeable difference between sweep 1 and sweep 10 is that in the latter, this value is reached almost from the start of the hydrodynamic regime. In engines in service, the components will be well run-in and the results from sweep 10 will therefore be more relevant. The running conditions of the journal bearing test rig are reasonably relevant for those occurring during normal operation of a buss engine, at least in terms of rotational speed and oil temperature.

However, one concern about the results provided by the test can be the relatively low load. With the load used, a 2 MPa specific contact pressure (specific pressure: load divided by projected area) is reached. However, in an actual engine, the journal bearings often experience specific pressures above 100 MPa due to dynamic loading from the combustion process and local pressures can reach 300 MPa [51–53]. However, for a full combustion cycle the average pressure will be substantially lower. It has also been shown that at start-stop conditions or low engine speeds (below 500 min^{-1}) contact pressures between 0 and 10 MPa can occur[54]. Taking into account that urban buses on operation could spend more than 40 % of the time idling[55], the friction coefficient differences found during the test are relevant even when the contact pressure value is lower than expected at engine full load conditions.

3.4. WAM machine results

After carrying out the proposed test plan described in section 2.4.1, the friction coefficient for the two oils under different entrainment speeds, SRR's, and temperatures can be seen in Figure 12.

All the plots have shown the expected behavior of these "μ-slip" curves, with a linear increase in friction coefficient with SRR's, followed by a non-linear region and then a maximum value due to the limiting shear stress of the oil. Then the friction decreases as the SRR increases mostly due to thermal softening of the lubricant. From the plots it is clear that the friction coefficient decreases when the 5W30 engine oil is used, the entrainment speeds increases and, once the local maximum of friction coefficient is reached and the curve enters into the thermal zone, when the

SRR increases.

3.4.1. The effect of LVEO on friction coefficient

As it was mentioned previously, the friction coefficient for the 5W30 oil has been lower in all test scenarios. However, the magnitude of these friction differences due to oil viscosity oscillate depending on the other parameters: temperature, SRR and entrainment speed. Accordingly to the behavior seen in Figure 12, it is obvious that friction reduction with the 5W30 oil is greater at 80 °C than 40 °C.

3.4.2. CNG bus cam and tappet

As seen in Figure 12, oil viscosity played a key role on the friction coefficient during the test and as it can be seen in Figure 13 the difference in percentage tends to remain steady after certain SRR is reached. This is when the thermal region has been reached and the oil thinning due to thermal effects is evident[41]. At 80°C the friction coefficient difference between oil formulations is higher than at 40°C. It is also noticeable that, unlike at 40°C, as entrainment speed increases from 2.5m/s to 4.0 m/s, the friction coefficient differences in percentage at different SRR present similar values, indicating that a pronounced increase in entrainment speeds could not be traduced into greater friction coefficient differences between reference and candidate oils at engine temperatures (see Figure 13). In the table 11 some of the characteristics of the cams used in this engine can be seen.

Given the fact that the actual cam profile is unknown, it was assumed that it follows a modified cycloidal cam profile which is commonly used in

Nominal diameter [mm]	48
Max height [mm]	56.52
Valve lift [mm]	8.52
Admission event angle [°]	115
Exhaust event angle [°]	123.5

Table 11: Cam characteristics

order to reduce sudden acceleration changes in the valve, being commonly applied in the automotive engines. The profile of cams used in automotive applications normally follow the DRRD pattern (dwell, rise, return, dwell). This periods are described by three curves; the cam base, the flank and the nose. The equations that describes the valve lift, speed and acceleration are the following:

$$S = L_i + L \left[\frac{\theta}{\beta} - \frac{1}{2\pi} \sin \left(\frac{2\pi\theta}{\beta} \right) \right] \quad (6)$$

$$V = \omega \frac{L}{\beta} \left[1 - \cos \left(\frac{2\pi\theta}{\beta} \right) \right] \quad (7)$$

$$A = \omega^2 \frac{2\pi L}{\beta} \sin \left(\frac{2\pi\theta}{\beta} \right) \quad (8)$$

Taking into account that $L_i = 0$ or 8.52 , $L = \pm 8.52$, and θ and β depending on the cam event angle and the actual cam angle, this equations can be solved for the different engine speeds during engine operation. As the engine has a Cam-tappet interface in the valvetrain, the kinematic analysis shown by Kushwahu [44] are used (see Figure 14). In that analysis the tappet spin is ignored and the entrainment speed is described as:

$$U_e = \frac{1}{2}\omega(R_o + S + 2J_\theta) \quad (9)$$

where R_o is the base radius, S is the valve lift at a given cam angle (given by the equation 6) and J_θ which is the geometric acceleration of the tappet given by the cam angle variation.

$$J_\theta = \frac{d^2 S}{d\theta^2} \quad (10)$$

Using the equations 3,7, 9 and 10, and the geometric known values of the cam, the tappet speed (Figure 15), the entrainment speed (Figure 16) and SRR were calculated for this specific contact using different speeds found during CNG engine operation. This calculations are valid for the admission cam, which was chosen since its event angle is narrower, hence the peak speeds were expected to be more critical than for the exhaust cam, having both the same nose height.

As it can be seen in Figure 15, assuming no spin in the tappet, the speed will have only a vertical component. This is determined by the cam profile and the engine speed in this case from 500 min^{-1} to 2200 min^{-1} .

In the calculated values of the entrainment speed performance differs strongly from the tappet speed. This is mainly due the action of the geometric acceleration of the tappet given by the cam angle variation.

The entrainment speed performance can be divided in two main sections; one, at the cam circular base where it is constant and given by the camshaft speed and the flank and nose sections, where the entrainment speed depends on the instantaneous radius of curvature at the contact point. As it can be seen in Figure 16, during the circular base of the cam, the entrainment speed

value is lower than the lowest value measured during the parametric study in the WAM Machine. However, it can be assumed from the performance of the oils shown in Figure 13, that the friction coefficient differences between the candidate and reference oil in the CNG engine were high, specially at normal operation temperatures. The Slide to Roll Ratio in this case corresponds to pure sliding.

For the second section, where the action of the flank makes the entrainment speed to increase rapidly, following the patterns of the geometric acceleration of the tappet. As it can be seen, and accordingly with the values found in the literature for this type of valvetrain design [44, 56–60], the entrainment speed does not exceed 2.5 m/s if the suggested cam profile is used. From the results shown in Figure 12, it is expected that during engine operation, when the tappet is lifted by the cam flank and nose and the entrainment speed increases the friction coefficient experience a reduction. From Figure 12, where the difference of friction coefficient between the two oils is depicted it can be seen that the reduction given by the use of an oil of lower viscosity diminishes in percentage. At lower entrainment speeds the difference between the oils is higher, however there is still a difference specially at 80°C. In the case of the Slide to Roll Ratio, similarly to section one, the value corresponds to pure sliding, taking into account that the speed in the direction parallel to tappet surface will be given by the cam rotational speed and the instantaneous radius. Even when the values measured for SSR in the WAM machine only reached mixed rolling and sliding conditions ($SRR \approx 1$) it can be said that the performance in terms of friction coefficient differences would be similar to the one found

at pure sliding since the thermal friction regime is reached even before a SRR value of 1 in the WAM, and with even higher values of SRR this regime will prevail with a continuous reduction in friction due to additional thermal softening of the lubricant.

4. Summary & Conclusions

- A significant difference in friction coefficient was detected for the less viscous oil using in the Cameron-Plint reciprocating machine.
- Given the Cameron-Plint limitations, only reverse operation points could be measured. However, the results supports the results of the fleet tests over the fuel consumption reduction effect of LVEO.
- The friction coefficient reduction due the use of 5W30 oil is more pronounced at 20 N of load and higher entrainment speeds. Hence, Heavy-Duty vehicles with working cycles with these kind of low load and high speed operating points are more likely to reduce fuel consumption with a LVEO.
- The high speed was the factor that maximize the effect of friction reduction of the 5W30 engine oil (6.727 % reduction).
- Extreme loads could prevent the benefits of low viscosity engine oils over fuel consumption as it was demonstrated in the ANOVA analysis. At 150 N the difference between 5W30 and 10W40 is almost negligible.
- Journal Bearing Test Rig results showed reductions as large as 8 % in friction coefficient under the hydrodynamic lubrication regime in

journal bearings. This difference in friction coefficient is almost steady for the whole engine speed range after the elements are run-in.

- The 5W30 oil proved to give lower friction coefficient values at entrainment speeds and slip values similar to those found in a Heavy Duty engine valvetrain.
- The results of the fleet test regarding fuel consumption benefits and the absence of wear, can be used by the fleet managers and final users to make a decision on whether or not use LVEO.
- On the other hand, tribometers tests proven to be useful to find friction coefficient differences in tribo-contacts similar to those found in the engine, even with OEM spare part as for the Cameron-Plint case. However, it is not possible to say that the behavior seen in those tests would be exactly the same in the engine due differences in operating conditions as relative speed, loads, geometries and so on. In order to complete a profile of a new formulation it would be necessary to validate the results with homologation tests as the M111 fuel economy test and the ASTM D7589.

Acknowledgments

The authors wish to express their gratitude to the Spanish Ministerio de Economía y competitividad Dirección General de Investigación Científica y Técnica for supporting the EFICOIL project (TRA2015-70785-R), the Colombian "Departamento Administrativo de Ciencia, Tecnología e

Innovación Colciencias” (C646-2014) and the Norrbottens Research council for financial support.

- [1] European Commission, Road transport: Reducing CO₂ emissions from vehicles, URL http://ec.europa.eu/clima/policies/transport/vehicles/index_en.htm, 2014.
- [2] K. Holmberg, P. Andersson, N. O. Nylund, K. Mäkelä, A. Erdemir, Global energy consumption due to friction in trucks and buses, *Tribology International* 78 (2014) 94–114, ISSN 0301679X, doi:10.1016/j.triboint.2014.05.004, URL <http://linkinghub.elsevier.com/retrieve/pii/S0301679X14001820>.
- [3] F. Payri, J. M. Desantes, *Motores de Combustión Interna Alternativos*, Reverté, Barcelona, ISBN 978-84-291-4802-2, 2005.
- [4] D. Taraza, N. Henein, W. Bryzik, Friction Losses in Multi-Cylinder Diesel Engines, SAE Technical Paper 2000-01-0921 (724), doi:10.4271/2000-01-0921., URL <http://digitallibrary.sae.org/content/2000-01-0921>.
- [5] A. Comfort, An Introduction to Heavy-Duty Diesel Engine Frictional Losses And Lubricant Properties Affecting Fuel Economy Part I, SAE Technical Paper 2003-01-3225 doi:10.4271/2003-01-3225, URL <http://digitallibrary.sae.org/content/2003-01-3225>.
- [6] W. W. Pulkrabek, *Engineering fundamentals of the internal combustion engine*, vol. 126, Prentice Hall, New Jersey, 2nd

- edition edn., ISBN 0131405705, doi:10.1115/1.1669459, URL <http://gasturbinespower.asmedigitalcollection.asme.org/article.aspx?articleid=2004>.
- [7] R. C. Coy, Practical applications of lubrication models in engines, *Tribology International* 31 (10) (1998) 563–571, ISSN 0301679X, doi:10.1016/S0301-679X(98)00077-2.
- [8] D. Hörner, Recent trends in environmentally friendly lubricants, *Journal of Synthetic Lubrication* 18 (4) (2002) 327–347, ISSN 0265-6582, doi:10.1002/jsl.3000180407, URL <http://doi.wiley.com/10.1002/jsl.3000180407>.
- [9] C. Calwell, Fuel Savings Possibilities from Low Viscosity Synthetic Motor Oils, in: International Energy Agency, Paris, 2005.
- [10] M. J. Souza De Carvalho, P. Rudolf Seidl, C. R. Pereira Belchior, J. Ricardo Sodr, Lubricant viscosity and viscosity improver additive effects on diesel fuel economy, *Tribology International* 43 (12) (2010) 2298–2302, ISSN 0301679X, doi:10.1016/j.triboint.2010.07.014.
- [11] G. Fontaras, E. Vouitsis, Z. Samaras, Experimental Evaluation of the Fuel Consumption and Emissions Reduction Potential of Low Viscosity Lubricants, SAE Technical Paper 2009-01-1803 .
- [12] B. Dohner, H. Umehara, T. Kanako, M. Yamashita, Development of Novel Friction Modifier Technology Part 2 : Vehicle Testing, SAE Paper (2011-01-2126) (2011) 1495–1500, doi:10.4271/2011-01-2126.

- [13] V. Macián, B. Tormos, S. Ruiz, L. Ramírez, J. de Diego, In-Use Comparison Test to Evaluate the Effect of Low Viscosity Oils on Fuel Consumption of Diesel and CNG Public Buses, SAE Technical Paper (2014-01-2794), doi:10.4271/2014-01-2794.
- [14] National Research Council, Technologies and Approaches to Reducing the Fuel Consumption of Medium- and Heavy-Duty Vehicles, Tech. Rep., National Academy of Sciences, Washington D.C., doi:10.17226/12845, URL <http://www.nap.edu/catalog/12845>, 2010.
- [15] M. Boyer, Improving Fuel Economy. The next challenge for engine oils., in: UEIL International Congress, Vienna, 2010.
- [16] W. van Dam, P. Kleijwegt, M. Torreman, G. Parsons, The Lubricant Contribution to Improved Fuel Economy, SAE Technical Paper 2009-01-2856 doi:10.4271/2009-01-2856.
- [17] W. van Dam, P. Kleijwegt, M. Torreman, G. Parsons, The Lubricant Contribution to Improved Fuel Economy, in: SAE Technical Paper 2009-01-2856, doi:10.4271/2009-01-2856, 2009.
- [18] W. van Dam, T. Miller, G. M. Parsons, C. Oronite, C. Llc, C. Way, Y. Takeuchi, The Impact of Lubricant Viscosity and Additive Chemistry on Fuel Economy in Heavy Duty Diesel Engines, SAE Technical Paper 2011-01-2124 ISSN 19463952, doi:10.4271/2011-01-2124.
- [19] P. Andersson, Piston ring tribology A literature survey VTT Industrial Systems, Tech. Rep., VTT Industrial Systems, Helsinki University, Internal Combustion Engine Laboratory, 2002.

- [20] J. J. Truhan, J. Qu, P. J. Blau, A rig test to measure friction and wear of heavy duty diesel engine piston rings and cylinder liners using realistic lubricants, *Tribology International* 38 (3) (2005) 211–218, ISSN 0301679X, doi:10.1016/j.triboint.2004.08.003, URL <http://linkinghub.elsevier.com/retrieve/pii/S0301679X04001586>.
- [21] J. J. Truhan, J. Qu, P. J. Blau, The effect of lubricating oil condition on the friction and wear of piston ring and cylinder liner materials in a reciprocating bench test, *Wear* 259 (7-12) (2005) 1048–1055, ISSN 00431648, doi:10.1016/j.wear.2005.01.025.
- [22] J. Jocsak, The Effects of Surface Finish on Piston Ring-pack Performance in Advanced Reciprocating Engine Systems, Master thesis, Massachusetts Institute of Technology, 2005.
- [23] O. M. E. Smith, In-Cylinder Fuel and Lubricant Effects on Gasoline Engine Friction, Ph.d. thesis, The University of Leeds, 2007.
- [24] M. Kapsiz, M. Durat, F. Ficici, Friction and wear studies between cylinder liner and piston ring pair using Taguchi design method, *Advances in Engineering Software* 42 (8) (2011) 595–603, ISSN 09659978, doi:10.1016/j.advengsoft.2011.04.008, URL <http://linkinghub.elsevier.com/retrieve/pii/S0965997811000895>.
- [25] A. Spencer, E. Y. Avan, A. Almqvist, R. S. Dwyer-Joyce, R. Larsson, An experimental and numerical investigation of frictional losses and film thickness for four cylinder liner variants for a heavy duty diesel engine, *Proceedings of the Institution of Mechanical*

- Engineers, Part J: Journal of Engineering Tribology 227 (12) (2013) 1319–1333, ISSN 1350-6501, doi:10.1177/1350650113491244, URL <http://pij.sagepub.com/lookup/doi/10.1177/1350650113491244>.
- [26] S. C. Vladescu, A. V. Olver, I. G. Pegg, T. Reddyhoff, The effects of surface texture in reciprocating contacts - An experimental study, Tribology International 82 (PA) (2015) 28–42, ISSN 0301679X, doi:10.1016/j.triboint.2014.09.015, URL <http://dx.doi.org/10.1016/j.triboint.2014.09.015>.
- [27] M. K. A. Ali, H. Xianjun, L. Mai, C. Qingping, R. F. Turkson, C. Bicheng, Improving the tribological characteristics of piston ring assembly in automotive engines using Al₂O₃ and TiO₂ nanomaterials as nano-lubricant additives, Tribology International 103 (2016) 540–554, ISSN 0301679X, doi:10.1016/j.triboint.2016.08.011.
- [28] S. C. Vladescu, S. Medina, A. V. Olver, I. G. Pegg, T. Reddyhoff, Lubricant film thickness and friction force measurements in a laser surface textured reciprocating line contact simulating the piston ring-liner pairing, Tribology International 98 (2016) 317–329, ISSN 0301679X, doi:10.1016/j.triboint.2016.02.026.
- [29] C. Shen, M. M. Khonsari, The effect of laser machined pockets on the lubrication of piston ring prototypes, Tribology International 101 (2016) 273–283, ISSN 0301679X, doi:10.1016/j.triboint.2016.04.009, URL <http://dx.doi.org/10.1016/j.triboint.2016.04.009>.
- [30] M. Söderfjäll, A. Almqvist, R. Larsson, Component test

- for simulation of piston ring - Cylinder liner friction at realistic speeds, *Tribology International* 104 (2016) 57–63, ISSN 0301679X, doi:10.1016/j.triboint.2016.08.021, URL <http://dx.doi.org/10.1016/j.triboint.2016.08.021>.
- [31] D. W. Gebretsadik, J. Hardell, B. Prakash, Tribological performance of tin-based overlay plated engine bearing materials, *Tribology International* 92 (2015) 281–289, ISSN 0301679X, doi:10.1016/j.triboint.2015.06.014, URL <http://linkinghub.elsevier.com/retrieve/pii/S0301679X15002522>.
- [32] H. Adatepe, A. Bykloglu, H. Sofuoglu, An investigation of tribological behaviors of dynamically loaded non-grooved and micro-grooved journal bearings, *Tribology International* 58 (2013) 12–19, ISSN 0301679X, doi:10.1016/j.triboint.2012.09.009, URL <http://dx.doi.org/10.1016/j.triboint.2012.09.009>.
- [33] D. E. Sander, H. Allmaier, H. H. Pribsch, F. M. Reich, M. Witt, A. Skiadas, O. Knaus, Edge loading and running-in wear in dynamically loaded journal bearings, *Tribology International* 92 (2015) 395–403, ISSN 0301679X, doi:10.1016/j.triboint.2015.07.022, URL <http://dx.doi.org/10.1016/j.triboint.2015.07.022>.
- [34] Y. Zhang, I. Tudela, M. Pal, I. Kerr, High strength tin-based overlay for medium and high speed diesel engine bearing tribological applications, *Tribology International* 93 (2016) 687–695, ISSN 0301679X, doi:10.1016/j.triboint.2015.03.010, URL <http://dx.doi.org/10.1016/j.triboint.2015.03.010>.

- [35] M. Teodorescu, V. Votsios, H. Rahnejat, D. Taraza, Jounce and impact in cam-tappet conjunction induced by the elastodynamics of valve train system, *Meccanica* 41 (2) (2006) 157–171, ISSN 00256455, doi: 10.1007/s11012-005-1609-0.
- [36] M. Teodorescu, A multi-scale approach to analysis of valve train systems, in: H. Rahnejat (Ed.), *Tribology and Dynamics of Engine and Powertrain*, Woodhead Publishing, Oxford, 1st edition edn., ISBN 978-1-84569-361-9, 567–587, doi:10.1533/9781845699932.2.567, URL <http://linkinghub.elsevier.com/retrieve/pii/B978184569361950017X>, 2010.
- [37] M. Shirzadegan, A. Almqvist, R. Larsson, Fully coupled EHL model for simulation of finite length line cam-roller follower contacts, *Tribology International* 103 (2016) 584–598, ISSN 0301679X, doi:10.1016/j.triboint.2016.08.017, URL <http://dx.doi.org/10.1016/j.triboint.2016.08.017>.
- [38] ACEA, ACEA European Oil Sequences 2016, Tech. Rep. 32, ACEA, URL http://www.acea.be/uploads/news_documents/ACEA_European_oil_sequences_2016.pdf, 2016.
- [39] V. Macián, B. Tormos, S. Ruíz, L. Ramírez, Potential of low viscosity oils to reduce CO2 emissions and fuel consumption of urban buses fleets, *Transportation Research Part D: Transport and Environment* 39 (2015) 76–88, ISSN 13619209, doi:10.1016/j.trd.2015.06.006.

- [40] SAE International, Internal Combustion Engines: Piston Rings Coil Spring Loaded Oil Control Rings, Tech. Rep. 724, SAE International, URL http://standards.sae.org/j2003_200806/, 2008.
- [41] M. Björling, R. Larsson, P. Marklund, E. Kassfeldt, EHL friction mapping - The influence of lubricant, roughness, speed and slide to roll., Proceedings of the Institution of Mechanical Engineers, Part J: Journal of Engineering Tribology. 225 (7) (2011) 671–681, doi:10.1177/1350650111403363, URL https://pure.ltu.se/portal/files/4792209/NordTrib2010_0060_paper.pdf.
- [42] D. Dowson, Elastohydrodynamic lubrication, in: Tribology and Dynamics of Engine and Powertrain: Fundamentals, Applications and Future Trends., Woodhead Publishing, Oxford, 1st edition edn., ISBN 978-1-84569-361-9, 1059, 1970.
- [43] R. Gohar, M. Safa, Measurement of contact pressure under elastohydrodynamic lubrication conditions, in: Tribology and dynamics of engine and powertrain: Fundamentals, applications and future trends, Woodhead Publishing, Oxford, 1st edition edn., ISBN 9781845693619, 222–245, doi:10.1533/9781845699932.2.284, 2010.
- [44] M. Kushwaha, Tribological issues in cam-tappet contacts, in: H. Rahnejat (Ed.), Tribology and Dynamics of Engine and Powertrain, Woodhead Publishing, Oxford, 1st edition edn., ISBN 9781845693619, 545–566, doi:10.1533/9781845699932.2.545, URL <http://linkinghub.elsevier.com/retrieve/pii/B9781845693619500168>, 2010.

- [45] J. Claret-tournier, Tribological Analysis of Injection Cams Lubrication in Order To Reduce, Tech. Rep., University of Halmstad, Halmstad, 2007.
- [46] V. Macián, B. Tormos, S. Ruiz, G. Miró, Low viscosity engine oils: Study of wear effects and oil key parameters in a heavy duty engine fleet test, Tribology International 94 (2016) 240–248, ISSN 0301679X, doi:10.1016/j.triboint.2015.08.028, URL <http://dx.doi.org/10.1016/j.triboint.2015.08.028>.
- [47] Y. Park, B. Weimer, J. Baxter, M. Roeth, Confidence Report: Low-Viscosity Engine Lubricants., Tech. Rep., North American Council for Freight Efficiency. NACFE., 2016.
- [48] G. W. Stachowiak, A. W. Batchelor, Engineering Tribology, Elsevier Butterworth - Heinemann, Oxford, 3rd edition edn., ISBN 9780750678360, doi:10.1016/B978-075067836-0/50018-3, URL <http://www.sciencedirect.com/science/article/pii/B9780750678360500183>, 2005.
- [49] E. Fuentes, K. Kanase, Relevance of Lubrication Regimes in the Study of Bearing Wear, in: P. Lakshminarayanan, N. S. Nayak (Eds.), Critical Component in Heavy Duty Engines, chap. 12, John Wiley & Sons, INC., Singapore, 1st edition edn., ISBN 978-0-470-82882-3, 199–252, 2011.
- [50] Cannon, Cannon HTHS Series II, URL <https://www.cannoninstrument.com/Image/GetDocument/492?language=en,> ????

- [51] M. D. Haneef, R. B. Randall, Z. Peng, Wear profile prediction of IC engine bearings by dynamic simulation, *Wear* 364-365 (2016) 84–102, ISSN 00431648, doi:10.1016/j.wear.2016.07.006, URL <http://dx.doi.org/10.1016/j.wear.2016.07.006>.
- [52] N. Marina, E. Ovchinnikova, Analysis of Performance Criteria of Boosted Diesel Engine Slide Bearings, *Procedia Engineering* 150 (2016) 45–51, ISSN 18777058, doi:10.1016/j.proeng.2016.06.713, URL <http://linkinghub.elsevier.com/retrieve/pii/S1877705816312504>.
- [53] D. E. Sander, H. Allmaier, H. H. Pribsch, F. M. Reich, M. Witt, T. Füllenbach, A. Skiadas, L. Brouwer, H. Schwarze, Impact of high pressure and shear thinning on journal bearing friction, *Tribology International* 81 (2015) 29–37, ISSN 0301679X, doi:10.1016/j.triboint.2014.07.021, URL <http://dx.doi.org/10.1016/j.triboint.2014.07.021>.
- [54] D. E. Sander, H. Allmaier, H. H. Pribsch, M. Witt, A. Skiadas, Simulation of journal bearing friction in severe mixed lubrication - Validation and effect of surface smoothing due to running-in, *Tribology International* 96 (2016) 173–183, ISSN 0301679X, doi:10.1016/j.triboint.2015.12.024, URL <http://dx.doi.org/10.1016/j.triboint.2015.12.024>.
- [55] T. Brightman, S. Girnary, M. Bhardwa, Bus idling and emissions, Tech. Rep. September, Transport & Travel Research1, URL http://www.pteg.net/system/files/PTEGBusIdling_ResultsReportfinalv10.pdf, 2010.

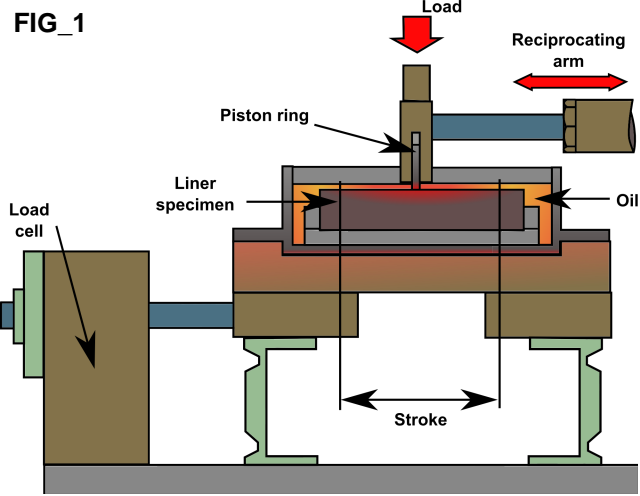
- [56] A. D. Ball, D. Dowson, C. M. Taylor, Cam and follower design, Tribology Series 14 (C) (1989) 111–130, ISSN 01678922, doi:10.1016/S0167-8922(08)70186-X.
- [57] G. Zhu, Valve trains - Design Studies, Wider Aspects and Future Developments, in: C. Taylor (Ed.), Engine Tribology, Elsevier, Amsterdam, 1st edition edn., 183–211, doi:10.1016/S0167-8922(08)70012-9, URL <https://www.elsevier.com/books/engine-tribology/taylor/978-0-444-89755-8>, 1993.
- [58] C. M. Taylor, Valve Train - CAM and Follower: Background and Lubrication Analysis, in: C. Taylor (Ed.), Tribology Series, vol. 26, Elsevier, Amsterdam, 1st edition edn., 159–181, doi:10.1016/S0167-8922(08)70011-7, 1993.
- [59] Q. Chang, P. Yang, J. Wang, Q. Chen, Influence of temperature on cam-tappet lubrication in an internal combustion engine, Frontiers of Mechanical Engineering in China 2 (4) (2007) 489–492, ISSN 16733479, doi:10.1007/s11465-007-0085-8.
- [60] J. Guo, W. Zhang, D. Zou, Investigation of dynamic characteristics of a valve train system, Mechanism and Machine Theory 46 (12) (2011) 1950–1969, ISSN 0094114X, doi:10.1016/j.mechmachtheory.2011.07.014, URL <http://dx.doi.org/10.1016/j.mechmachtheory.2011.07.014>.

Figure captions

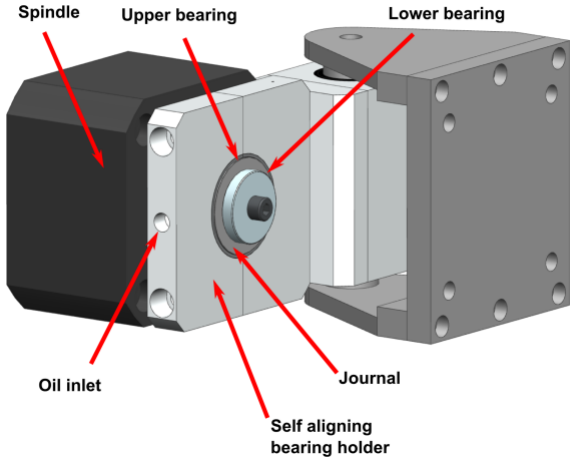
- Figure 1. Cameron-Plint TE77 test configuration.
- Figure 2. Journal bearing test setup.
- Figure 3. WAM machine, ball-on-disc test device.
- Figure 4. Fuel consumption differences on the fleet test for the CNG buses.
- Figure 5. ANOVA results for the Oil Control Ring (OCR).
- Figure 6. Test results for the different rings.
- Figure 7. Load and frequency effects over friction coefficient of Oil Control Ring (OCR).
- Figure 8. Stribeck curves of the OCR for different loads.
- Figure 9. Oil and frequency effects over friction coefficient of Oil Control Ring (OCR).
- Figure 10. Oil and load effects over friction coefficient of Oil Control Ring (OCR).
- Figure 11. Friction coefficient results for Journal Bearing Test Rig.
- Figure 12. Friction coefficient results for WAM machine tests.
- Figure 13. Friction coefficient differences between 10W40 and 5W30 oils at 40°C and 80°C and different entrainment speeds.

- Figure 14. Cam-Tappet contact diagram.
- Figure 15. Tappet speed at different engine speeds.
- Figure 16. Entrainment speed in the admission Cam-tappet contact at different engine speeds.

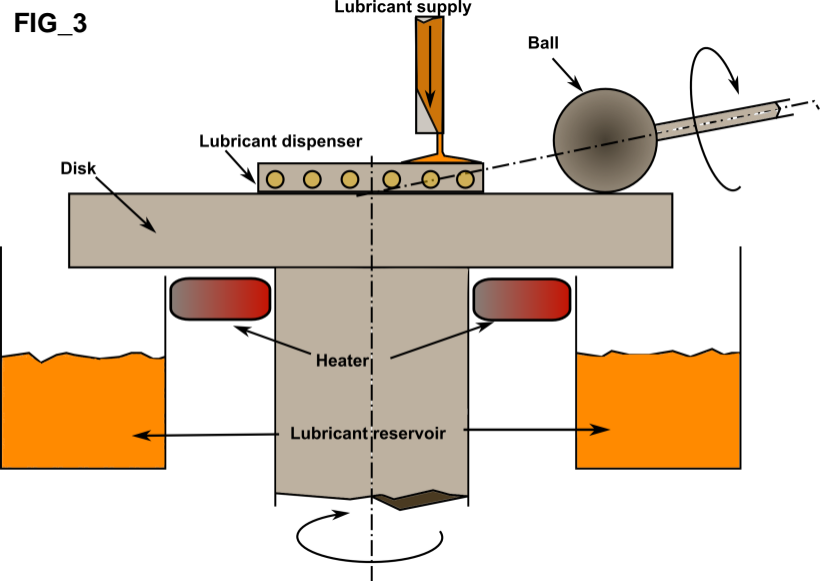
FIG_1



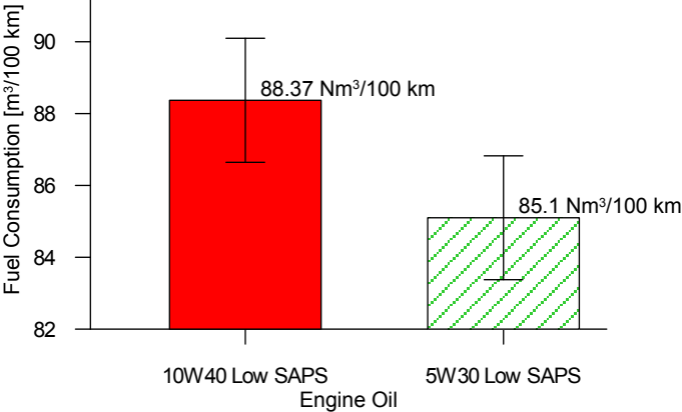
FIG_2

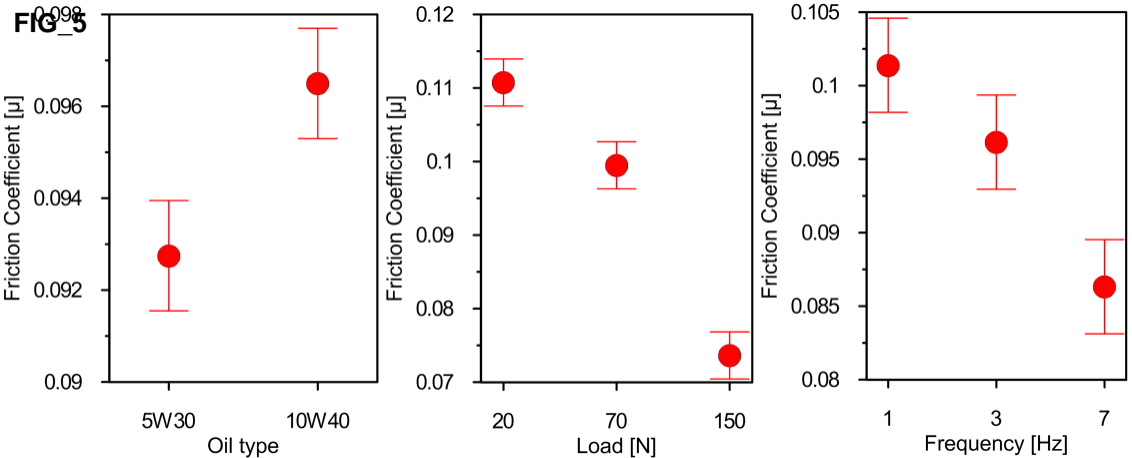


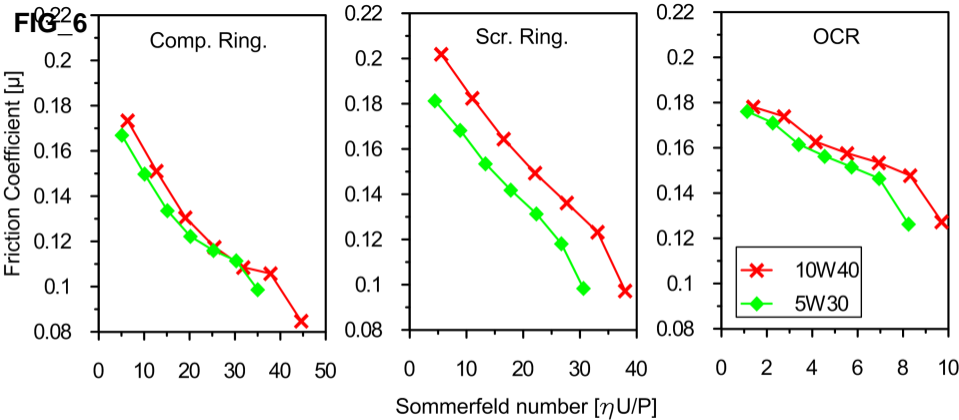
FIG_3



FIG_4







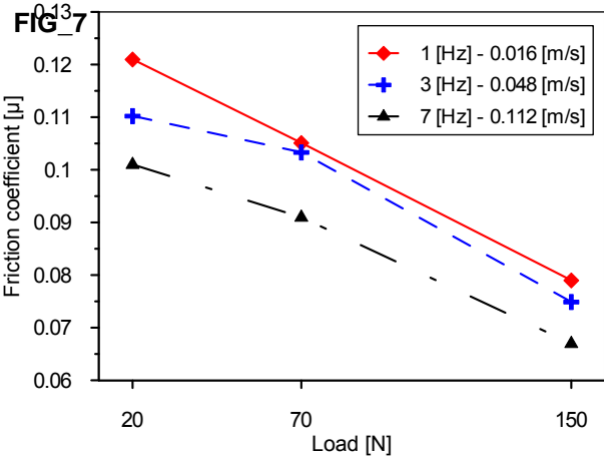
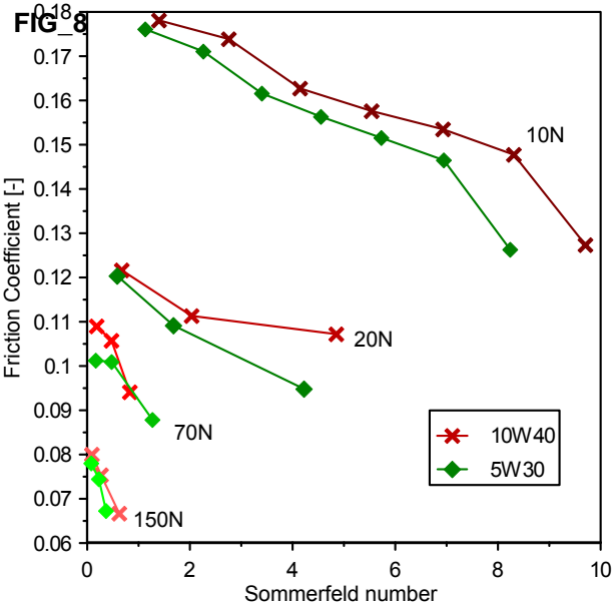
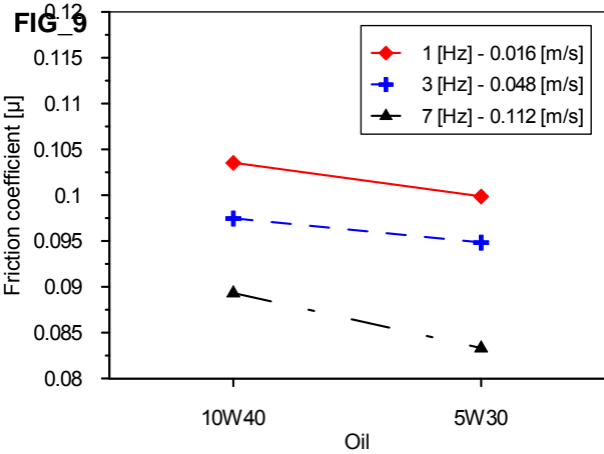


FIG 8



FIG_9

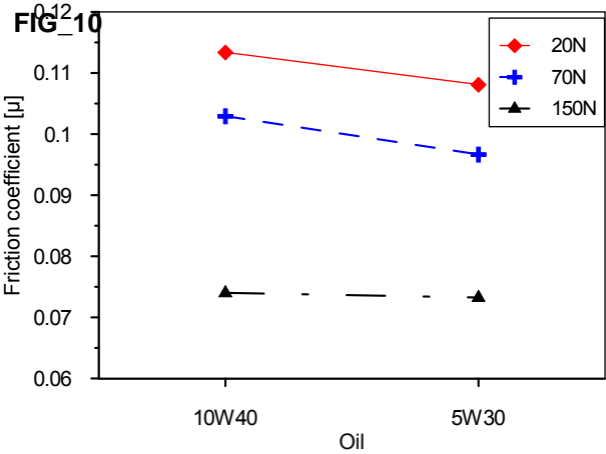
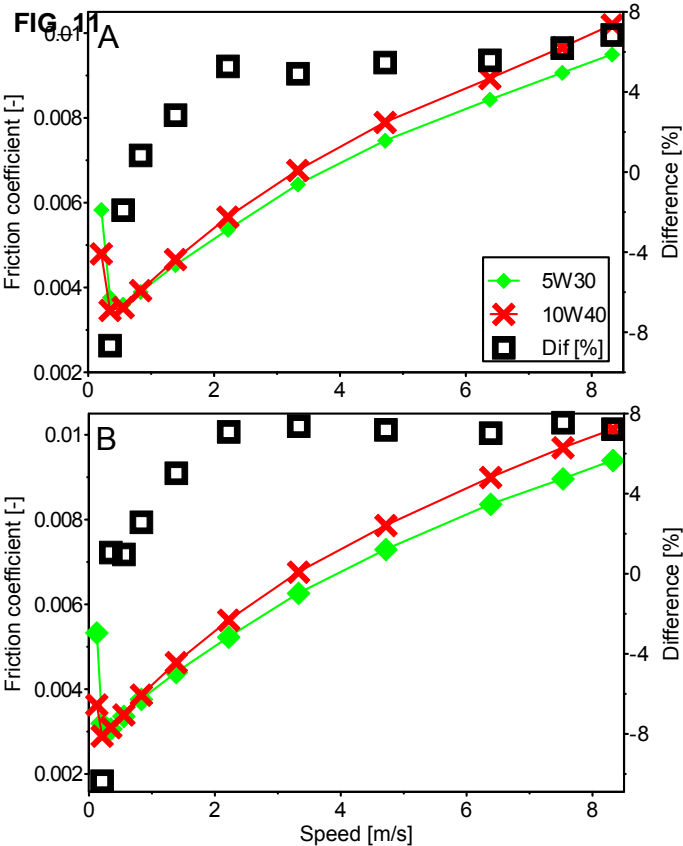
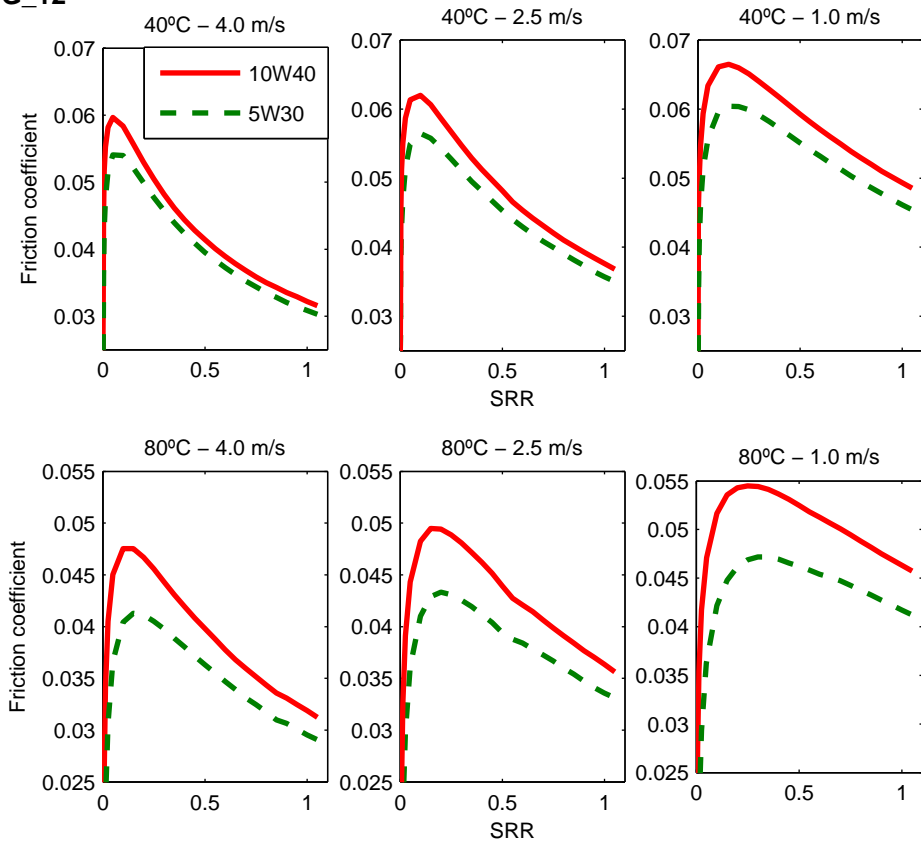
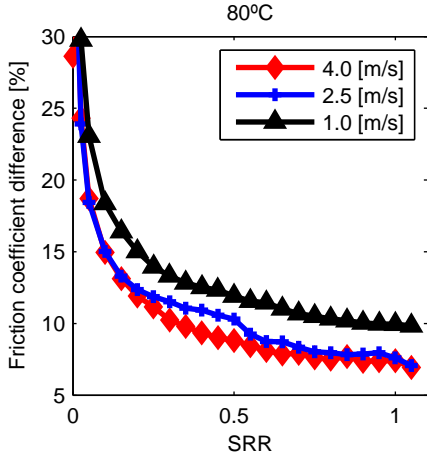
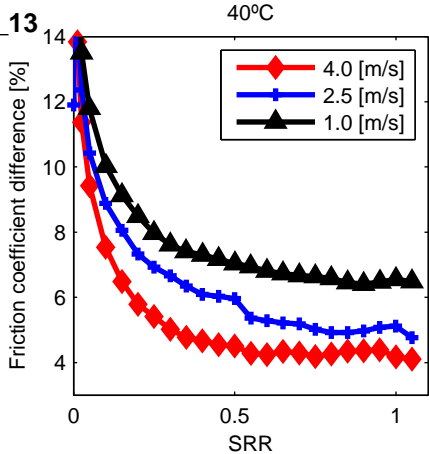
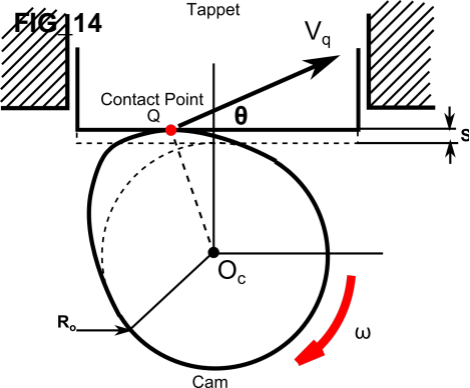


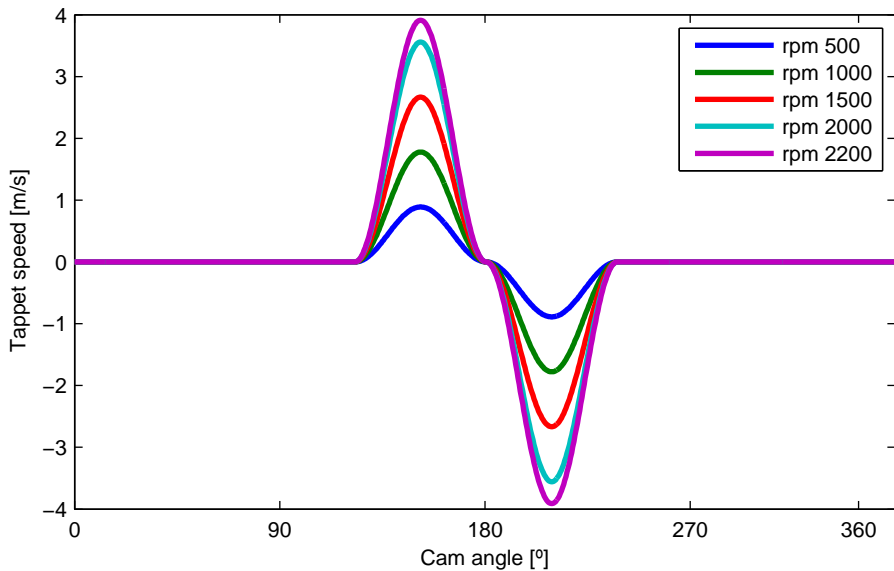
FIG. 11

FIG_12

FIG_13





FIG_15

FIG_16